Electrochemical and Solid-State Letters, **6** (12) A260-A264 (2003)
0013-4651/2003/6(12)/A260/5/$7.00 © The Electrochemical Society, Inc.

Reversible Behavior of $K_2Fe(VI)O_4$ in Aqueous Media

In Situ ^{57}Fe Mössbauer and Synchrotron X-Ray Spectroscopy Studies

S. Ghosh,[a] W. Wen,[a] R. C. Urian,[a] C. Heath,[a,*] V. Srinivasamurthi,[a,] W. M. Reiff,[a] S. Mukerjee,[a,*,z] V. Naschitz,[b] and S. Licht[b,*]**

[a]*Department of Chemistry, Northeastern University, Boston, Massachusetts 02115, USA*
[b]*Department of Chemistry, Technion-Israel Institute of Technology, Haifa 32000, Israel*

The chemistry of the Fe(VI) compound, K_2FeO_4, was investigated in aqueous potassium hydroxide electrolyte for its potential use in secondary storage systems. High charge storage K_2FeO_4 material was synthesized using alkaline hypochlorite oxidation of ferric nitrate and characterized by *in situ* X-ray diffraction and Mössbauer spectroscopy. The discharge-charge profile of the cathode, measured *vs.* a zinc anode, was semiquantitatively correlated with changes in Fe^{6+}/Fe^{3+} ratio and the nature of structural transformation at each stage by *in situ* Mössbauer and *in situ* synchrotron X-ray diffraction spectroscopy. The data in conjunction with the charge-discharge profile clearly indicates the rechargeability of K_2FeO_4 with a charge efficiency of about 36% of the total current passed under the prevailing experimental conditions. These results are potentially important to the design of Fe^{6+} compound analogs for use in secondary energy storage systems.
 [DOI: 10.1149/1.1621751]

Manuscript submitted April 12, 2003; revised manuscript received June 27, 2003. Available electronically October 1, 2003.

Batteries find wide application in various devices, including mobile electronics, medical implants, transportation, and their need for further improvement drives the development of electrochemical energy storage technology. Currently, commercial secondary storage batteries are comprised of nonaqueous electrolyte-based lithium ion (or polymer), aqueous alkaline electrolyte-based nickel-metal hydride, nickel-cadmium, and others, such as the lead-acid technology. Most primary batteries correspond to the alkaline Zn/MnO_2 system. The common denominator in the current state-of-the-art aqueous (metal hydride) and nonaqueous (Li-ion) batteries is the limitation of cathode capacity. In the nonaqueous rechargeable Li-ion system, a typical capacity of ~150 mAh g^{-1} is achieved for the $LiCoO_2$[1] cathode in comparison to the anodic capacity of 3860 and 760 mAh g^{-1} for lithium and $Li_{2.6}Co_{0.4}N$ anodes,[2] respectively. A cathodic capacity of approximately 120-140 mAh g^{-1} is typically achieved for $LiMn_2O_4$ spinel albeit with concern about its durability as a function of cycling due to Jahn-Teller related lattice distortion. In primary batteries such as Zn/MnO_2 the charge capacity of MnO_2 (308 mAh g^{-1}) is also limited as compared to that of the zinc anode (820 mAh g^{-1}).

The motivation for finding high-capacity cathode materials is therefore a common theme in the context of battery chemistry. In this context, Fe(VI) charge storage (so-called super-iron) compounds present an interesting future cathode material for both aqueous primary alkaline and nonaqueous secondary battery applications.

Although Fe(VI) species have been known for more than a century, their chemistry and potential application as battery electrode materials, remains relatively unexplored.[3-5] This results from ready decomposition of FeO_4^{2-} during synthesis in aqueous medium, the rate of decomposition being accelerated in the presence of metal cations such as Ni^{2+} or Co^{2+}. The first reports of the use of $MFeO_4$ ($M = K_2$, Sr, and Ba) in aqueous primary and secondary alkaline cells as well as in nonaqueous primary cells were those by Licht *et al.*[6-9] Dried K_2FeO_4 is stable over time in different chemical environments.[7] The solubility of this salt is minimum in highly concentrated potassium hydroxide solution and can be further reduced by adding $Ba(OH)_2$.[9] The relative insolubility of K_2FeO_4 has dual advantages of preventing (*i*) solution-phase decomposition and (*ii*) cathode diffusion to the anode, thereby preventing chemical self-discharge. Hence this material has attracted recent attention as a candidate cathode material for both primary and secondary alkaline battery configurations.

In aqueous phase, the full charge capacity can be described by reactions such as

$$FeO_4^{2-} + 5/2H_2O + 3e^- \rightarrow 1/2Fe_2O_3 + 5OH^- \qquad [1]$$

Coulombic efficiencies, greater than 70% of the theoretical charge capacity, have been achieved with K_2FeO_4 electrodes.[6] These results have suggested a three-electron reduction mechanism involving Fe^{6+} to Fe^{3+}. This is based on the comparison of the experimentally and theoretically calculated coulombic charge capacity with a cutoff voltage of 0.6 V *vs.* zinc, which nullifies the contribution from reduction of Fe^{3+} to lower (valence) oxidation states of iron.

In aqueous KOH electrolyte, the observed extended reversibility of the Fe(VI) cathode in a super-iron metal hydride cell has been ascribed to a complementary proton insertion mechanism such as[6]

$$K_2FeO_4 + xH_2O + xe^- \rightleftharpoons H_xK_2FeO_4 + x\ OH^{-1} \qquad [2]$$

Combining Reaction 2 with the known anode reaction (such as a metal hydride), a super-iron/metal hydride battery may be discharged according to

$$K_2FeO_4 + MH_x \rightleftharpoons H_xK_2FeO_4 + M \qquad [3]$$

where MH_x = charged metal hydride anode.

In prior studies, there has been no direct spectroscopic proof of a three-electron redox couple involving Fe^{6+}/Fe^{3+}. Further, the chemistry of the reversibility of this redox couple remains unknown. All prior reports[6] are based purely on electrochemical data without insight as to the nature of the microscopic structural transformations involved. The question of reversibility is also unclear in the context of the type of structural transformation and its associated Fe valence change. This is especially important as the prior data on reversibility[6] involved a composite material.

The goal of this communication is to provide an initial understanding of the details of chemical change, corresponding to the charging and discharging process of Fe^{6+} based batteries. In this endeavor, basic electrochemical data of the discharge/charge and subsequent discharge of an electrode containing potassium ferrate (K_2FeO_4) is correlated with simultaneous data from *in situ* Mössbauer and synchrotron X-ray diffraction (XRD) measurements. Therefore, this article is designed to provide the first insight into the electrochemical behavior of these materials and as such acts as a

* Electrochemical Society Active Member.
** Electrochemical Society Student Member.
z E-mail: smukerje@lynx.neu.edu

forerunner of a more detailed publication which will describe structural transformations and changes in the local environment of Fe from the perspective of electronic (valence states, etc.) as well as short-range atomic order (coordination sphere, bond distances, etc.) using *in situ* synchrotron X-ray absorption fine structure (XAFS) and variable-temperature Mössbauer spectroscopy.

Experimental

K_2FeO_4 of 99% purity was synthesized, using analytical grade reagents, from the alkaline hypochlorite oxidation of ferric nitrate according to the equation[8]

$$2Fe(NO_3)_3 \cdot 9H_2O + 3KOCl + 10KOH \rightarrow 2K_2FeO_4 + 3KCl + 23H_2O + 6KNO_3 \quad [4]$$

K_2FeO_4 was precipitated from the solution by the addition of excess solid potassium hydroxide. Product purity was determined by the chromite method described in detail elsewhere.[7]

High resolution *in situ* XRD spectra were acquired at the National Synchrotron Light Source (NSLS) in the Brookhaven National Laboratory (BNL), Upton, NY, using beam line X-7A. Details of the beam-line optics and data analysis are given elsewhere.[10] Monochromatic radiation with a wavelength of 0.7038 Å was obtained using a channel-cut double-crystal Ge(111) monochromator. A linear position-sensitive detector[11] was used to collect the data.

A specially designed *in situ* cell was used for these measurements, which was similar to those described earlier.[12] In this cell (half-cell) the counter and reference were Zn foil (0.1 mm thick), with a commercial cellulose separator (Duracell) and the working electrode sandwiched with 13.5 M KOH. The data were collected in the transmission mode using a special Teflon window in the *in situ* spectroelectrochemical cell. Details of these measurements and the nature of measurements in the transmission mode using synchrotron X-ray are given elsewhere.[12]

The performance of the super-iron cathode was evaluated using both a coin-type as well as an *in situ* spectroelectrochemical cell with a zinc metal anode. The zinc foil, 0.1 mm thick, was purchased from Alfa Aesar of 99.995% purity. The cathode composite electrode was formed by mixing 90 mg of K_2FeO_4, with 50 mg of 1-2 μm graphite (Aldrich chemicals, USA) using 13.5 M KOH as the electrolyte. The total capacity of this cathode electrode corresponded to 36.54 mAh, based on a three-electron reduction. The galvanostatic discharge experiment of K_2FeO_4 was performed at 23°C using an Arbin cycler at a rate of C/36.5. The subsequent charge/discharge steps were performed at C/36.5 and C/73 rates, respectively.

The *in situ* Mössbauer spectra (constant acceleration mode) were determined at ambient temperature using a specially modified cell based largely on our synchrotron spectroelectrochemical cell design. The source was 25 mCi ^{57}Co in a Rh lattice. Velocity calibration of the spectrometer was based on the hyperfine splitting of α-Fe at room temperature.

Consecutive 4 h Mössbauer scans were made throughout the charging-discharging process with no equilibration steps. The data therefore represent spectra, which are dynamic (changing during the measurement process).

Results and Discussion

Figure 1 shows the XRD pattern of K_2FeO_4 in an electrode at the open-circuit condition in a spectroelectrochemical cell prior to discharge. This spectrum was indexed using Cerius2 software (Accelrys, USA) to a single-phase orthorhombic structure with the space group *Pnma*. The calculated lattice parameters for this compound were $a = 10.3429$ Å, $b = 7.7020$ Å, and $c = 5.8629$ Å, respectively. These are in good agreement with prior literature.[3]

Figure 2 shows the XRD patterns of the cathode material in different stages of discharge. As evident from Fig. 2b, the X-ray powder-diffraction pattern of the final discharge product shows complete absence of new peaks. The peaks shown in Fig. 2b are those

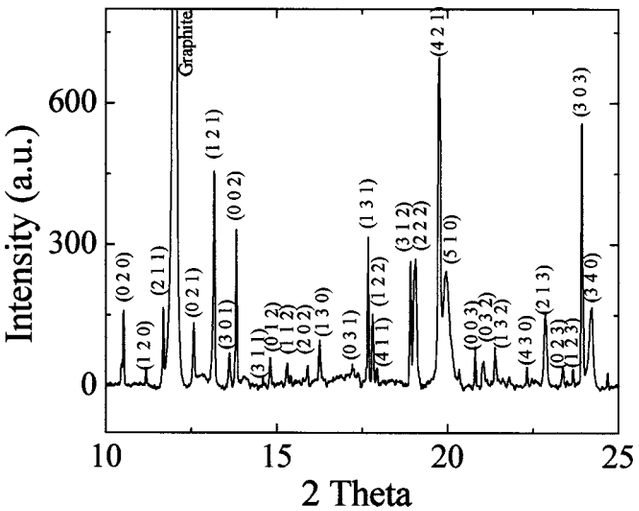

Figure 1. The XRD pattern of potassium ferrate recorded with λ = 0.7038 Å. This represents the data for a fresh electrode at open-circuit condition in a spectroelectrochemical cell prior to discharge. Data taken at beam line X-7A, at NSLS (BNL).

from residual ferrate material which have been indexed with the corresponding *hkl* values for K_2FeO_4. This indicates that the final discharge product is completely amorphous. Most diffraction peaks of potassium ferrate are missing because of the interference from the amorphous discharge product and the possibility of preferred orientation in the final discharged state. However a more detailed characterization of this process using *in situ* X-ray absorption spectroscopy (XAS) is in progress to determine the nature of the local environment around Fe; this will better elucidate the final structure of the discharge product.

The *in situ* synchrotron X-ray powder diffraction pattern after charging for 21.8 h (represented by a charge capacity of 242.5 mAh/g or 85.6% of the discharge capacity) is shown in Fig. 2e. The lattice parameters, obtained after indexing the charged spectrum using powder indexing (Cerrius2) are $a = 10.36070$ Å,

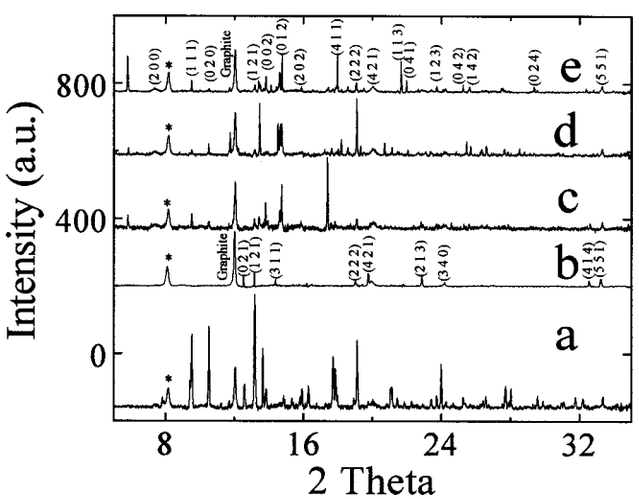

Figure 2. *In situ* Synchrotron XRD patterns of K_2FeO_4 cathode at different stages of charge and discharge. (a) Pure K_2FeO_4 before discharge; (b) end of discharge at a cutoff potential of 0.6 V *vs.* Zn; recharged for (c) 10 h, 111 mAh/g, (d) 15 h, 167 mAh/g, and (e) 21.8 h, 242.5 mAh/g. The beam line (X7A at NSLS, BNL) was tuned at λ = 0.7038 Å. The diffraction peak corresponding to the stainless steel cell feature is indicated with *.

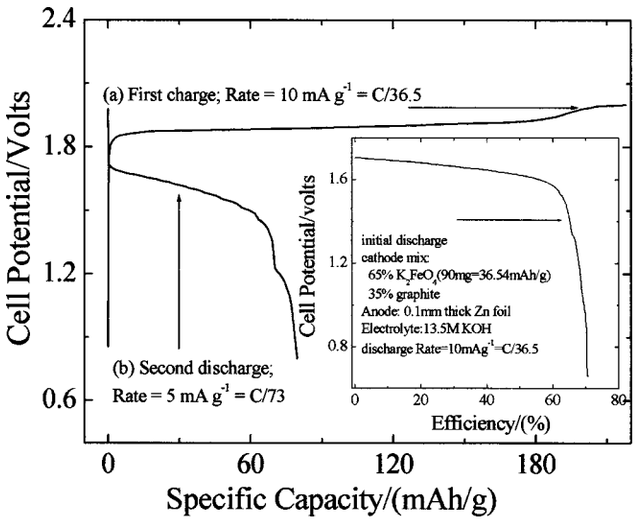

Figure 3. Galvanostatic charge-discharge profile of Zn-K_2FeO_4 alkaline battery measured in both coin type (inset) and *in situ* spectroelectrochemical cell (main plot). Based on the loading, the maximum theoretical capacity of the working electrode was 36.5 mAh. The first discharge (inset) and charge (main plot) were at the rate of C/36.5, followed by the second discharge (main plot) at C/73 rate.

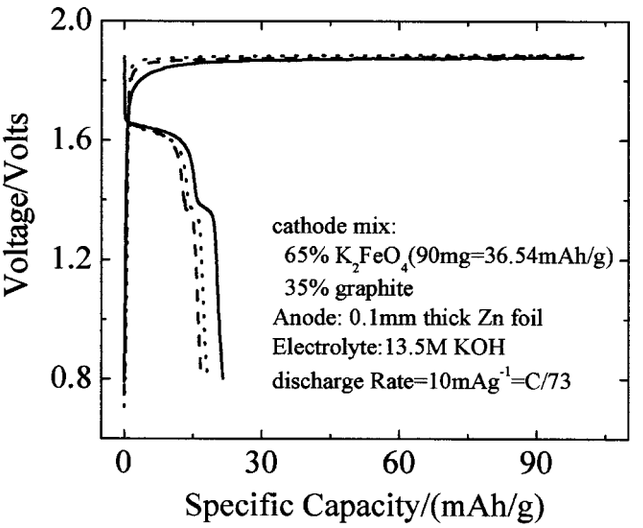

Figure 4. Galvanostatic charge-discharge profile of Zn-K_2FeO_4 alkaline battery measured in coin-type cell. Based on the loading, the maximum theoretical capacity of the working electrode was 36.5 mAh. The cell is cycled at C/73 rate. First cycle (solid line), second cycle (dashed line), third cycle (dotted line).

b = 7.70702 Å, and c = 5.86238 Å corresponding to an orthorhombic unit cell. These lattice parameters are close to those of the starting material whose corresponding lattice parameters were a = 10.3429 Å, b = 7.7020 Å, and c = 5.8629 Å, respectively. Almost all the peaks are indexed with those of potassium ferrate. However, a few peaks of the starting potassium ferrate are not observed in spectrum e. There are two possible reasons for this phenomenon. The first is that the potassium ferrate formed in the charged state has a different preferred orientation from that of the starting material. The second is the possibility of interference due to the presence of a significant amount of Fe^{3+}. It is also noticed that a new peak at a 2-theta angle near 6° appeared in spectra c-e. The exact origin of this peak is unknown at this moment.

Figure 3 (inset) presents the discharge profile of a K_2FeO_4 cathode using coin-type cell configuration with a zinc anode and a cathode, which was a homogeneous mixture of potassium ferrate and 1 to 2 μ graphite with 13.5 M KOH as electrolyte. Figure 3 (inset) represents the initial discharge profile at the rate of C/36.5. The open-circuit potential of the cathode *vs.* Zn was 1.75 V, with the cell transitioning to a plateau of approximately 1.65 V. The initial discharge profile showed a steady decay to a potential of approximately 1.5 V, which corresponds to around 60% of the theoretical capacity (406 mAh/g based on three-electron reduction). This decay exhibits relatively low polarization losses indicating that the charge-transfer resistance in this discharge step until 1.5 V does not change significantly. Beyond this the discharge profile shows a sharp inflection toward lower potentials with a very small plateau at approximately 1.3 V perhaps suggesting a relatively unstable $Fe^{4+/3+}$ transition state. This implies a two-step discharge behavior for Fe^{6+}. The first step, where a smooth transformation to Fe^{4+} is indicated based primarily on capacity of the plateau at 1.65 to 1.5 V (approximately a two-electron reduction). The second step is relatively unstable and represents approximately 10% of the observed capacity. The total discharge capacity up to a cutoff potential of 0.65 V was 25.55 mAh, which represents a discharge efficiency of 70% based on the calculated theoretical capacity of 406 mAh/g (using a three-electron reduction).

Figure 3 (main plot) shows the subsequent charge data at the same rate (C/36.5) to a cutoff potential of 2.0 V. This data represents those collected in the *in situ* spectroelectrochemical cell used for X-ray and Mössbauer spectra. The choice of cutoff potential was made to avoid any potential problems related to corrosion of the electrode material, especially the graphitic carbon. However, as evident from the charge profile, the charge capacity was 21.8 mAh, which represents approximately 85% of the discharge capacity or a specific capacity of 217 mAh/g. The charge profile shows a very rapid transition to a plateau of 1.88 V that remains relatively flat until a specific capacity of approximately 180 mAh/g (or 16 mAh) is reached followed by a small inflection toward the cutoff potential of 2.0 V. This flat plateau indicates a different transformation compared to the discharge profile. The rapid transition to 1.88 V followed by a flat plateau may indicate the possibility of the presence of intermediate species in various oxidation states.

Figure 3 (main plot) also shows the second discharge step, which is represented by the data measured in the *in situ* spectroelectrochemical cell after the first charge step. A cutoff potential of 0.8 V was chosen. The observed capacity in the second discharge step corresponds to a specific capacity of 76 mAh/g corresponding to 35% of the charge capacity. This second discharge step exhibits a similar profile to the first one. The initial plateau however has a higher slope, which is likely due to presence of a considerable amount of residual Fe^{3+}, a poor electronic conductor. The subsequent cycles are shown in Fig. 4, where an efficiency of about 20% was achieved with a cutoff voltage of 0.8 V. Interestingly, the small plateau around 1.3 V, observed in the first discharge cycle, also appeared in all subsequent discharge cycles.

Figure 5a presents the *in situ* Mössbauer spectrum of K_2FeO_4 in the spectroelectrochemical cell before the discharge process. This spectrum corresponds to an open-circuit potential of 1.75 V, which was very stable for the duration of the measurement. Following this, the cell discharge was initiated with simultaneous measurement of Mössbauer data at various stages of cycling. The corresponding electrochemical data is shown in Fig. 3 (inset). Since the discharge rate was C/36.5, and each spectrum took 4 h, they therefore each represent 11% of the theoretical capacity. Comparison with the discharge data in Fig. 3 (inset) however shows a 70% discharge efficiency, which translates to an actual change of 15.6% during each Mössbauer scan. The initial spectrum, corresponding to the cell at open circuit prior to discharge, Fig. 5a, shows a single resonance line with an isomer shift of −0.72 mm/s at 298 K. This is in excel-

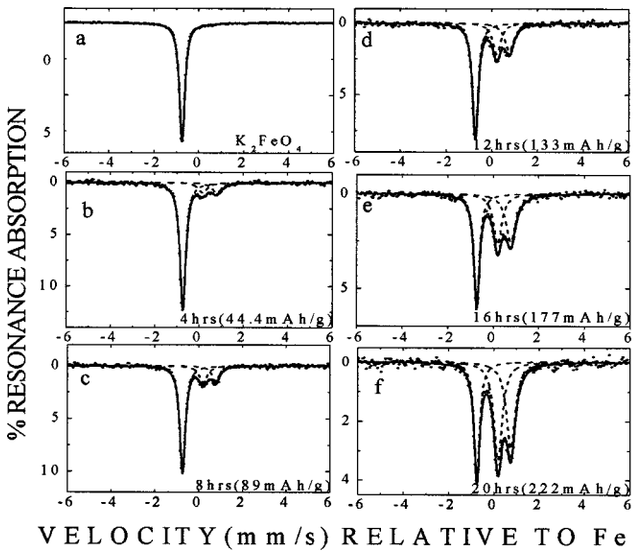

Figure 5. *In situ* Mössbauer spectra of Zn-K_2FeO_4 alkaline battery during the discharge process (a) data at open circuit. As a function of cell discharge after (b) 4 h, 44.44 mAh/g, (c) 8 h, 89 mAh/g, (d) 12 h, 133 mAh/g, (e) 16 h, 177 mAh/g, and (f) 20 h, 222 mAh/g.

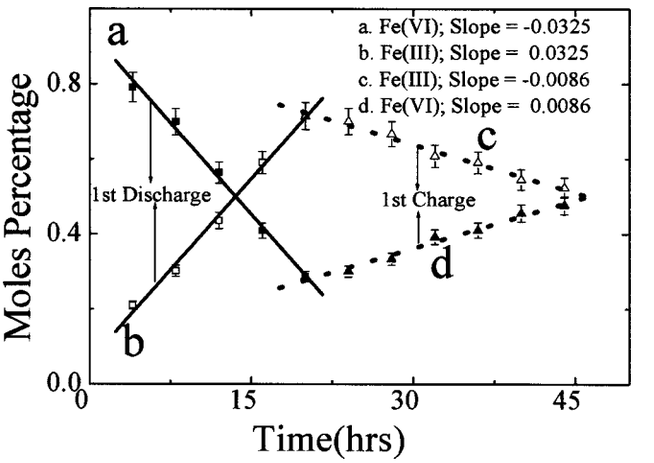

Figure 6. Percent moles (of Fe^{3+} and Fe^{6+}) *vs.* time plot using *in situ* Mössbauer data. (a and b) Fe(VI) and Fe(III) species in the first discharge cycle. (c and d) Fe(III) and Fe(VI) in the first charge cycle.

lent agreement with the literature[4] and confirms that our starting material is pure K_2FeO_4.

Figure 5b shows the *in situ* Mössbauer spectrum of the cathode after 4 h discharge when the cell voltage was around 1.65 V. The spectrum indicates an appearance of a doublet coincident with a decrease in the singlet intensity, *i.e.*, a lowering of the Fe^{6+} ion concentration. A subsequent spectrum, Fig. 5c after 8 h, represents an increase of this effect and provides a snapshot of the discharge profile at approximately 23% of the overall discharge (Fig. 3 inset). The spectra of the cell toward the end of the discharge step represented by Fig. 5d, e, and f clearly indicate the emergence of Fe^{3+} as the discharge product. The isomer shift of the doublet is 0.48 mm/s while the quadrupole splitting is 0.57 mm/s, parameters typical of high spin Fe^{3+} species.[4] However, there is no evidence of a Fe(IV) intermediate (transient or otherwise) in the Mössbauer spectroscopy time scale (~100 ns). In particular, the isomer shift and small quadrupole splitting effect (0.48 mm/s, 0.57 mm/s relative to Fe) of the limiting discharge product are fully consistent with high spin Fe(III). In view of the probable metal ligation, oxygen, both spin quintet (S = 2) Fe(IV) and spin triplet (S = 1) are ruled out. The former is expected[13] to exhibit a singlet Mossbauer spectrum with an isomer shift ~0.06 mm/s relative to Fe at ambient temperature as found[13] for $SrFeO_3$. The triplet form of Fe(IV)[14] also exhibits a substantially more negative isomer shift (0.22 mm/s relative to Fe) than found herein and is accompanied by a large electric field gradient/quadrupole splitting effect. It is clear that the single-line resonance of the K_2FeO_4 has not completely disappeared. This is also reflected by the coulombic efficiency of the cell that was around 70% of the theoretical value (inset Fig. 3). These data indicate that there is only ~30% of potassium ferrate left and generally are consistent with the Mössbauer results shown in Fig. 6.

Following the discharge step, the cell was charged against the zinc anode at a constant current at the rate of C/36.5 to a cutoff potential of 2.0 V *vs.* zinc metal (Fig. 3). As mentioned earlier, this charge step corresponded to 21.8 mAh, which, expressed as specific capacity, corresponds to 242 mAh/g. The charge pattern shows that the cell voltage increased very fast until 1.88 V *vs.* Zn. This was followed by a more steady increase to 2.0 V. As mentioned above, this recharge corresponds to 85.6% of the discharge capacity.

The corresponding *in situ* Mössbauer spectra during the charging process are shown in Fig. 7. They are consistent with reversibility of the Fe^{3+} to Fe^{6+} transformation. The series of spectra, each comprising a 4 h duration, indicate a steady decline in the Fe^{3+} species and the reverse transformation to Fe^{6+}. At the end of the charge step, the spectrum (after 24 h) indicates the presence of unconverted Fe^{3+}. Hence the cell is not completely reversible. This has implications for the second discharge behavior and subsequent cycling behavior.

The relative amount of Fe^{3+} and Fe^{6+} was determined using the integrated area under the corresponding Mössbauer peaks. Using the thin-absorber approximation, the area under each of the corresponding peaks (Fe^{3+}, Fe^{6+}) represents the product of the mole of each individual ion and the recoil-free factor. The recoil-free factors of K_2FeO_4 and the discharged product are not known and are assumed to be similar. The relationship between the percentages of the Fe species *vs.* time is presented in Fig. 6. These are linear plots, which suggest a single prime reaction for both charge and discharge. It is important to note that the slopes in the variation of each of the ions, corresponding to the first discharge profile, as represented by de-

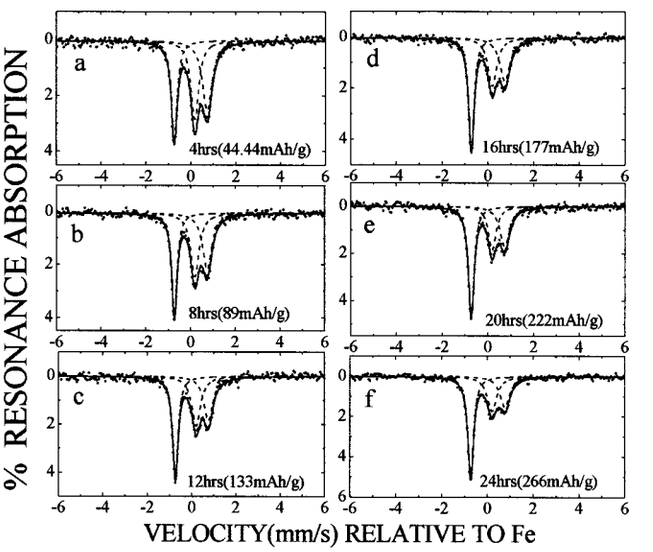

Figure 7. *In situ* Mössbauer spectra of Zn-K_2FeO_4 alkaline battery at different stages of charge (a) 4 h, 44.44 mAh/g, (b) 8 h, 89 mAh/g, (c) 12 h, 133 mAh/g, (d) 16 h, 177 mAh/g, (e) 20 h, 222 mAh/g, and (f) 24 h, 266 mAh/g.

crease of Fe(VI) and the concomitant increase in Fe(III), are the same (Fig. 6). This is also true for the charge cycle (Fig. 6). It suggests that the assumption of the recoil-free factors of the individual ions being similar is valid. However, comparison of the slopes between the discharge and charge data is different. The difference is approximately fourfold. The implication of this difference however is unclear.

Conclusion

The Mössbauer spectra at this stage do not provide clear insight into the exact identity of the Fe^{3+} product species. In previous (mostly speculative) work, a polymorph of FeOOH or Fe_2O_3[6] have been proposed. The latter and certain polymorphs of the former exhibit nuclear Zeeman split Mössbauer spectra (not observed herein) at ambient temperature for magnetic domain size $\geqslant$180 Å (18 nm).[15] This is the typical Mössbauer spectroscopy, manifestation of a bulk, 3d magnetically ordered solid. For particle size ~10 nm, the solid becomes a superparamagnet with concomitant vanishing of the magnetic hyperfine splitting of the Mössbauer spectra and coincidental broadening or even disappearance of its XRD pattern. The Fe^{3+} product's Mössbauer spectrum determined herein is that of a rapidly relaxing paramagnet. This result and its XRD data are fully consistent with an essentially amorphous Fe^{3+} product species. This aspect will be studied further in the context of low-temperature Mössbauer spectroscopy experiments where magnetic hyperfine splitting highly characteristic of various Fe^{3+} can be observed. Further, the short range atomic order around Fe studied using *in situ* XAS is expected to provide complementary structural information. We also plan to study the reversible behavior of the K_2FeO_4 cathode in nonaqueous medium, as it is compatible with a lithium anode.

Acknowledgment

The authors gratefully acknowledge startup grants from Northeastern University and support from the U.S. Department of Energy, Materials Science Division, for financial assistance in building and maintaining the National Synchrotron Light Source at Brookhaven National Laboratory (Upton, NY). S.L. is grateful for partial support from the Israel Science Foundation.

Northeastern University assisted in meeting the publication costs of this article.

References

1. J. M. Tarascon and M. Armand, *Nature (London)*, **414**, 359 (2001).
2. T. Shodai, Y. Sakurai, and T. Suzuki, *Solid State Ionics*, **122**, 85 (1999).
3. R. J. Audette, J. W. Quail, W. H. Black, and B. E. Robertson, *J. Solid State Chem.*, **8**, 43 (1973).
4. G. K. Wertheim and R. H. Herber, *J. Chem. Phys.*, **36**, 2497 (1962).
5. B. Wagner, D. Reinen, T. C. Brunold, and H. U. Guedel, *Inorg. Chem.*, **34**, 1934 (1995).
6. S. Licht, B. Wang, and S. Ghosh, *Science*, **285**, 1039 (1999).
7. S. Licht, V. Naschitz, L. Halperin, N. Halperin, L. Lin, J. Chen, S. Ghosh, and B. Liu, *J. Power Sources*, **101**, 167 (2001).
8. S. Licht, V. Naschitz, and S. Ghosh, *J. Phys. Chem. B*, **106**, 5947 (2002).
9. S. Licht, B. Wang, S. Ghosh, J. Li, and V. Naschitz, *Electrochem. Commun.*, **1**, 522 (1999).
10. http://neutrons.phy.bnl.gov/~powder/
11. G. C. Smith, *Synchrotron Radiat. News*, **4**, 24 (1991).
12. S. Mukerjee, T. R. Thurston, N. M. Jisrawi, X. Q. Yang, J. McBreen, M. L. Daroux, and X. K. Xing, *J. Electrochem. Soc.*, **145**, 466 (1998).
13. P. K. Gallagher, J. B. MacChesney, and D. N. E. Buchanan, *J. Chem. Phys.*, **2**, 2429 (1964).
14. W. M. Reiff, B. Dockum, and W. T. Oosterhuis, *J. Chem. Phys.*, **67**, 3537 (1977).
15. W. Kuendig, H. Boemmel, G. Constabaris, and R. H. Lindquist, *Phys. Rev.*, **142**, 327 (1966).